Detection of gold bearing rocks using aster data at Gabel Gharib, northeastern Desert, Egypt

Abd El Mohsen Gharieb[1], Abass Sharaky[2], Kholoud Mohamed Abdel Maksoud[2]

1- Nuclear Materials Authority, Cairo, Egypt.
2- Institute of African Research and Studies, Cairo University, Egypt.

* Corresponding Author: Kholoud.mohamedali@gmail.com

Received: 11 April 2013 / Accepted: 31 May 2013 / Published online: 3 June 2013

Abstract

The Gharib area is sited between latitudes 28º 10' 12" - 28º 01' 37" N and Longitudes 32º 55' 02" - 32º 38' 29" E, in the Eastern Desert- Egypt, covers an area 500 Km^2, this area is covered mainly by younger granites; The younger granite is considered as one of the most important basement rock due to its economic value, where it used in different purposes metallic purpose, and as raw material which are used for ornamental stones. Remote sensing is an important and useful tool for mapping and detection of alteration zones, which properly important for identifying ore deposits. ASTER imagery are reliable, accurate and of good ability to assist geologists in mineral exploration stages. Using image processing technique such as band rationing method (bands ratio 4/8, 4/2 and 8/9 used for hydrothermal alteration zones to detect gold occurrence, band ratios 4/5, 4/6 and 4/7 in RGB Show the discrimination of hydrothermal alteration and band ratios 5/7, 3/1 and 4/3 show the iron gossan an iron- bearing sulphide ore bodies where gold are enriched in this oxidation zone area). The hydrothermal alteration zones are detected in the South western side of the study area Gabel Gharib which located in the northern part in the Pan African Belt, and by using Classification methods such as SAM and MLC are used to make an up-to-date geologic map with scale 1:50,000. These methods Results in detecting gold mineralization in the study are also verified that the methods are fruitful and could be applicable elsewhere.

Keywords: ASTER, Gold, Pan-African, Gharib Mountain.

1- Introduction

Remote sensing technology displayed a great role in mineral investigation and prospecting of ores. The ASTER (the Advanced Space borne thermal Emission and Reflection Radiometer) imagery used provides accurate information. Reconnaissance of hydrothermal ore deposits exploration is linked to distinctive spectral properties of the image (Mars and Rowan, 2006; Di Tommaso and Rubinsten, 2007; Zhang *et al*., 2007; Kargi, 2007; Gabr *et al*., 2010). Geologists have an incredible opportunity to be a target potential for hydrothermal ore deposits with remote sensing data which has been enhanced after launching of ASTER.

ASTER is multispectral imaging sensor that measures reflected and emitted electromagnetic radiation from Earth's surface and atmosphere in 14 bands. These bands are divided into three groups; three visible and near infrared (VNIR) bands ranging in wavelength between 0.52 and 0.86 µm with spatial resolution of 15m; six bands of short wavelength infrared radiation (SWIR) ranging from 1.6 to 2.43 µm with spatial resolution of 30m; 5 thermal infrared radiation bands (TIR) range from 8.125- 11.65 µm in wavelength with spatial resolution 90m (Yamaguchi *et al*., 1999; Abrams, 2000). Chart 1 show the research method taken in to achieve the geologic map and band ratio maps .

Precambrian rocks occupy about one tenth of the land surface of Egypt. They form mountains terrains in southern Sinai and the Eastern Desert as well as small, low lying in lines in the southern parts of western Desert.

Figure 1) location map for the study area located in red spot.

The Eastern Desert is divided into three sectors: Northern Eastern Desert (NED), Central eastern Desert (CED) and the Southern eastern Desert (SED), the study area is located in the NED (Fig. 1), it could be reached by an asphaltic road (Shiekh Fadel- Ras Gharib road) 45 km to the west of Ras- Gharib city.

Harraz and El- Sharkwy, (1997) studied the Ras Gharib granitoid rocks and observed a remarkable trend of Mn enrichment in ilmenite, which indicate that the magmatic process is controlling Mn distribution in limonite. Mohamed *et al.* (1999) stated that the province of Ras Gharib district includes wide surface areas of granitoid rocks that occur in the form of separate plutons and large batholiths, the granitoid rocks can be divided mainly into a calc-alkaline suite of granodiorite, monzogranite and syenogranite, a trondhjemite suite, and an alkali granite suite. They also mentioned that granodiorite- monzogrnaite – syenogranite are widely distributed with moderate enrichment in the LREE and LILE, the trondhjemtic rocks are more silicic and occur as small irregular bodies into the granodiorite-monzogranite association. Mostafa and Bishta (2005) used Landsat ETM+, data for Gabel Gharib- Dara area in the northern part of the eastern desert of Egypt and applied the Geo- Analyst PCI EASI/PACE software to extract the lineaments digitally and correlating lineaments density maps (LDM) with aeroadiometry total count countor maps. They also mentioned that the studied granitic rocks are of high density in both lineament and lineament intersection. They also showed that younger granitic is the only rock unit which has been classified into four sub- lithologic units- G1, G2, G3 and G4. Bishta, (2006) studied Esh-ElMellaha area in the Northern part of the Eastern Desert by using the color raster aero-radiometric total count map with the interpreted lithologic and structural maps, he observed a radioactive anomalous in the studied area which are controlled by intersections of structural lineaments trending along N-S, NE- SW and WNW-ESE direction. It is clear that the previous authors have worked on the whole province in addition of rare remote sensing work have done on the selected area which make this work is worthy to do. The study area is known for quarrying purpose, and nothing mentioned about metallic mineralization, quarrying sites are present in the extreme south (Fig. 2) or above the area while metallic mineralization is out of sight, so this work is worthwihle in studying.

2- Geology of the study area

Pan-African granitoids occupy a significant portion of the Egyptian basement complex north of latitude 26º N. In 1979, Dixon mentioned that syn- to late tectonic granites cover 34.6% of the Northern Eastern Desert (NED) and 26.7% of the whole Eastern Desert (ED), while the younger post-tectonic granites occupy about 35% and 16.2% respectively. The region of interest is located in NED, where granitoid plutons cover a wide area of the surface exposure.

Most geological studies were mainly concentrated on the central and southern parts of the Eastern Desert and little is known about the north part. The study area is part of the northern extension of the late Proterozoic basement in the Eastern Desert of Egypt. (Mohamed *et al.*, 1999; Abdel Rahman, 1990, 1995; Abdel Rahman and Martin, 1990) proposed that the regional geological setting of this part of the Eastern Desert has changed from primitive oceanic island arc to continental margin setting during the Pan-African event; where The Pan-African orogenic cycle has long been recognized as a period of major crustal accretion, where continental, island, and oceanic terranes were brought together to form the crystalline basement of the Africa continent as part of late Neoproterozoic supercontinent (Urug, 1997), where some parts of the Pan-African orogeny are characterized by continental collisional tectonics (Burke and Sengor, 1987; Stern, 1994). Others are typical of accretionary orogens (Kroner *et al*., 1987 and Windley, 1992). This was followed by continental extension and rifting around the late Proterozoic- Paleozoic boundary. Accordingly, the alkaline granite (Gabel Gharib pluton) is considered as A-type granite formed in a rift environment after Pan-African orogeny (Abdel-Rahman and Martin, 1990).

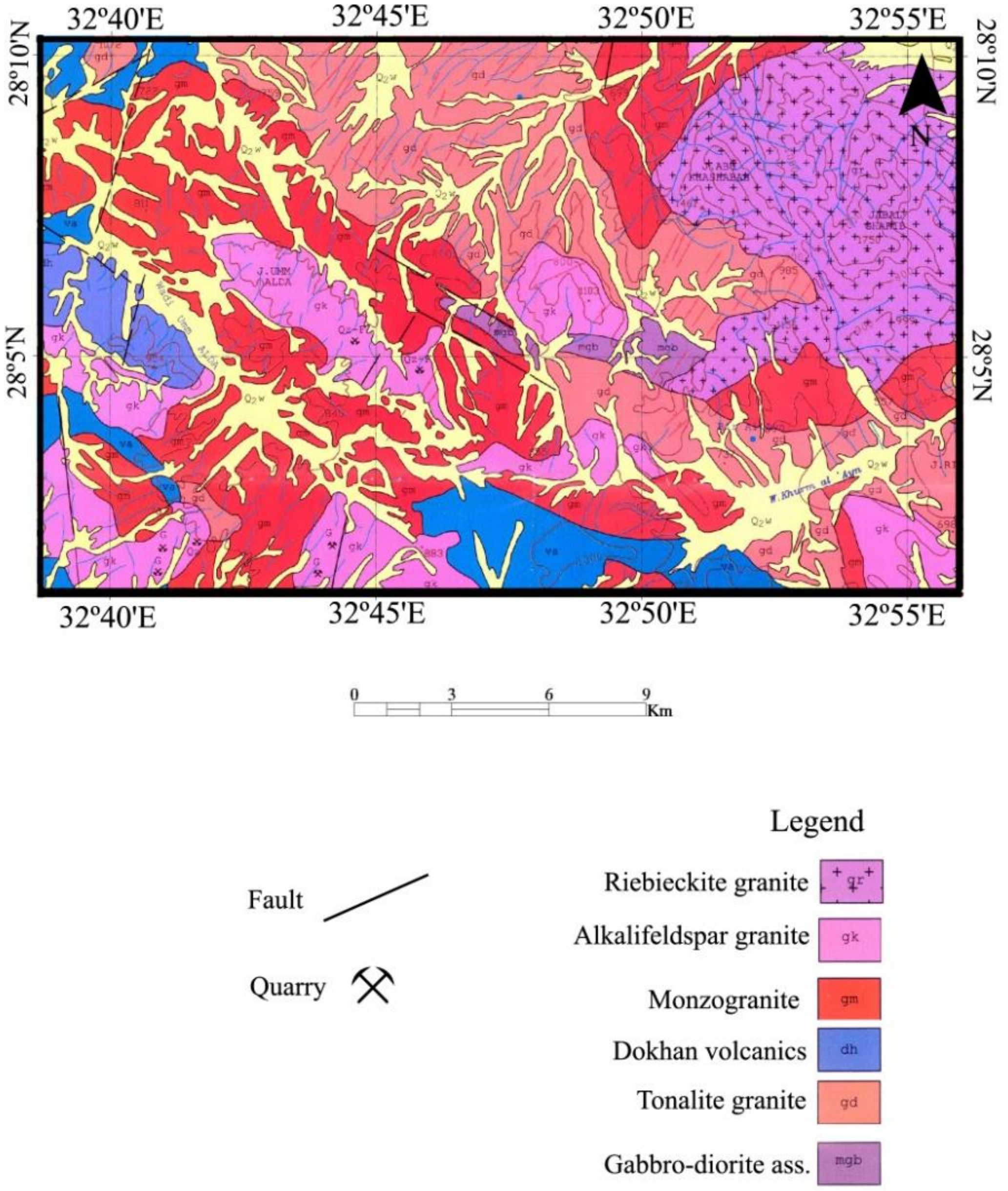

Figure 2) geologic map of study area (after geologic survey of Egypt. 1984).

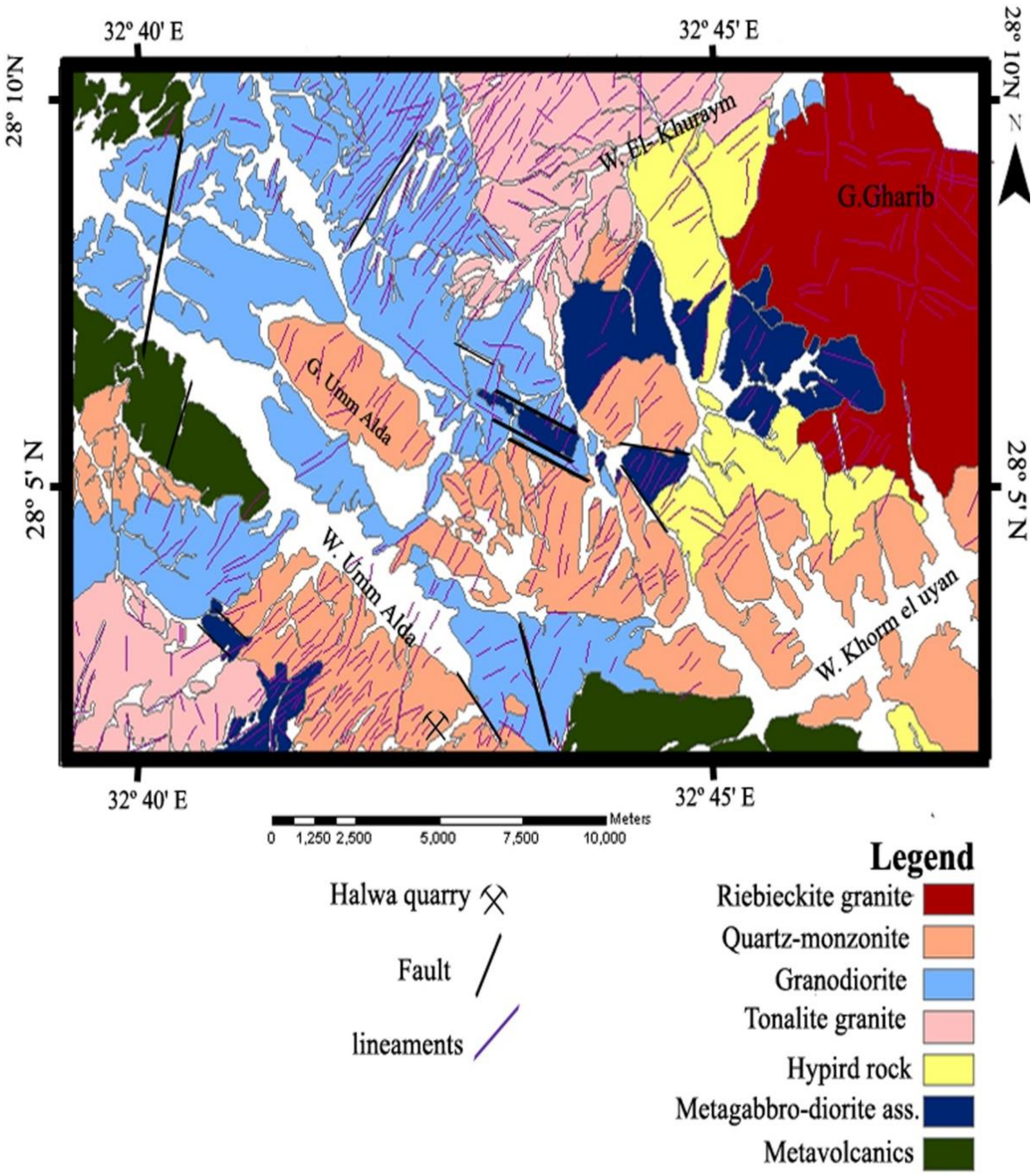

Figure 3) Up- to date geologic map.

The study area is considered as the beginning of the Pan-African belt, covered by Basement Complex. The area is occupied by different types of Calc-alkaline granites with metagabbro- diorite association, the calc-alkaline granites are intruded by numerous small felsic alkaline granitic intrusions. (Hegazy and El-Shazly, 2000). The selected area has rarely been investigated by previous authors especially in the field of geology and remote sensing.

The Geologic Survey of Egypt published a geologic map in 1984 (Conoco map) for the northern belt of the Eastern Desert including the study area (Fig. 2). This geologic map show that the selected area consists of 3 rock units which are arranged from youngest to oldest as; Riebeckite granite (Gabel Gharib), Alkalifeldspar granite, Monzogranite, Dokhan volcanic, Tonalite granite and Gabbro-diorite association.

Hume (1935) studied the northern granite of Gabel Gharib as alkali riebeckite granite, while (Nower *et al*., 1990) studied the younger granites of Egypt and classified Gabel Gharib as strongly A-ype alkali feldspar granite. The geologic map was modified and processed using ASTER data by classification method, SAM and by regulated field trip (Fig.3).

A new modification and nomenclature were observed in the field and confirmed by classification methods which are the metagabbro-diorite association, quartz monzonite and granodiorite.

An extension for the metagabbro diorite association was detected making a sharp contact with Gabel Gharib (riebeckite granite) which makes a doubt of mineralization zone in this area and it was (Fig. 4).

3- Remote sensing methodology

The remote sensing data used in this study are part of the cloud free scene level 1B ASTER data acquired on 2006. The image was brought through the Earth and Remote sensing Data Analysis Center (ERSDAC, Japan), and was pre-geo referenced to UTM Zone 36N with WGS-84 datum. The ASTER image was then stacked so that all 14 bands have the same 15×15 m pixel size and then clipped to the study area.

Later on after processing, the image was resampled. Nearest neighbor resample method was applied in order to prevent interpolation of the pixel values by using the nearest pixel values (Amer *et al*, 2010; Xianfeng, *et al*., 2007) show that the ASTER data were capable of mapping flood basalt, quartz-biotite gneiss, muscovite schist, granitic, volcanic, and metasedimentary rock units, also it shows excellent correlation with those on the reference geologic map, Four alteration minerals: alunite, kaolinite, muscovite and montmorillonite can be detected by subpixel unmixing analysis of the ASTER reflectance data. (Gulam and Kusky, 2010) used CEM technique in gold exploration and they found that The CEM technique, did not perform well in conditions because of the background signature is not easily detected, so it fails to indentify rare minerals (e.g. secondary iron-rich parts of the alteration), using CEM when there is no apparent difference between the target and background spectral signatures. (Amin *et al*., 2011) work on ASTER imagery to locate and enhance alteration zones associated with ore deposits and found that PCA, MNF and band rationing results in absolute correspond with previous workers.

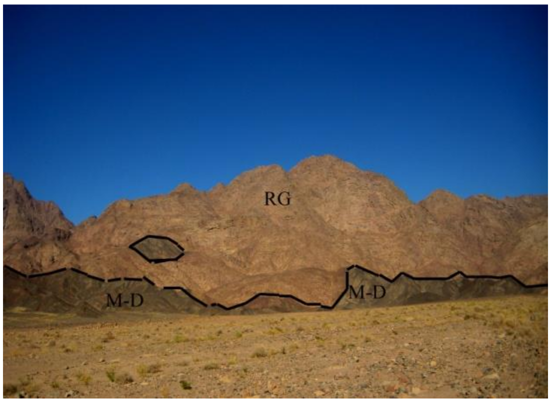

Figure 4: The Riebeckite granite (RG) intrudes sharply the metaggabro- diorite association (M-D).

Alteration is commonly forms a halo around the mineralization which probably is larger than the deposit itself. This halo is considered as the exploration target, the characterization of hydrothermal alteration is a key to locate the main flow zones of hydrothermal system which may lead to the recognition of mineral deposits (Rajesh, 2004).

3.1- Image Processing

The geologic map was modified after the following Image processes were made and these processes are:

Minimum Noise Fraction transformation (MNF)

Noise is common on multispectral images. Because it causes interference with the identification of materials and with the calculation of their abundance, it is necessary to eliminate it in order to obtain good spectra, (Gharieb, 2010). The MNF technique is used to reduce noise in multispectral images.Boardman and Kruse (1994) used MNF to determine the inherent dimensionality of image data, to segregate noise in the data and to reduce the computational requirements for subsequent processing. The MNF procedure is derived from PCA (principal component analysis) but it is like ordering of components according to image quality, (Gharieb, 2010).

The MNF procedure was examined on Resample data and three sub-system VNIR and SWIR and TIR separately, and the eigen values of the 14 output bands are shown in Table 1 with MNF eigenimages are shown in Figures 5 and 6. Eigenimages with near-unity eigen values (less than 1) are normally noise-dominated and usually excluded from the data as noise in order to improve the subsequent spectral processing (Jensen, 2005) The eigenvalues of the MNF are from 2.6 to 90.6 and these values to show a decrease in signal noise ratio.

All the eigenvalues greater than 1 so all 14 bands of the ASTER data were retained for subsequent data processing (Figs 5 and 6).

Table 1) The MNF eigenvalues of the 14 eigenimages for the ASTER data of Gharib area.

Bands	Eigen Values	Eigen values %	Cumulative %
1	90.31	37.00	37
2	51.68	21.00	58
3	17.33	7.00	65
4	13.94	5.67	70.67
5	12.87	5.23	76
6	11.50	4.67	80.57
7	10.50	4.27	84.84
8	9.92	4.03	88.87
9	8.54	3.47	92.34
10	5.43	2.20	94.54
11	4.33	1.79	96.30
12	3.68	1.49	97.79
13	3.64	1.48	99.27
14	2.06	0.83	100

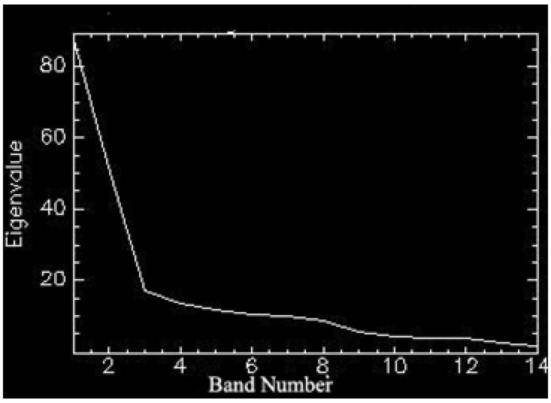

Figure 5) Degradation if the signal all along the MNF components.

3.3- Pixel Purity Index (PPI)

To reduce the number of pixels to be analyzed for endmembers determination and to facilitate the separation of pure materials from mixed ones. The PPI determine automatically the relative purity of the pixel from the higher order MNF eigenimages (Boardman, 1993; Boardman *et al*, 1995). The extreme pixels in each projection are recorded and the total number of times each pixel is marked as extreme is noted, a PPI is created in which the digital number (DN) of each pixel corresponds to the number of times that the pixel was recorded as extreme, (Gharieb, 2010). PPI image is formed in which the digital number (DN) of each pixel corresponds to the total number of times that the pixel was falling onto the ends of the unit vector in all projections. PPI was applied on the MNF image to select the most pure pixels, a 10,000 projection of the scatter plot and the threshold factor of 2.5 were applied on the data (Figs. 7 and 8). These were implemented to be used for *n*-dimensional visualization.

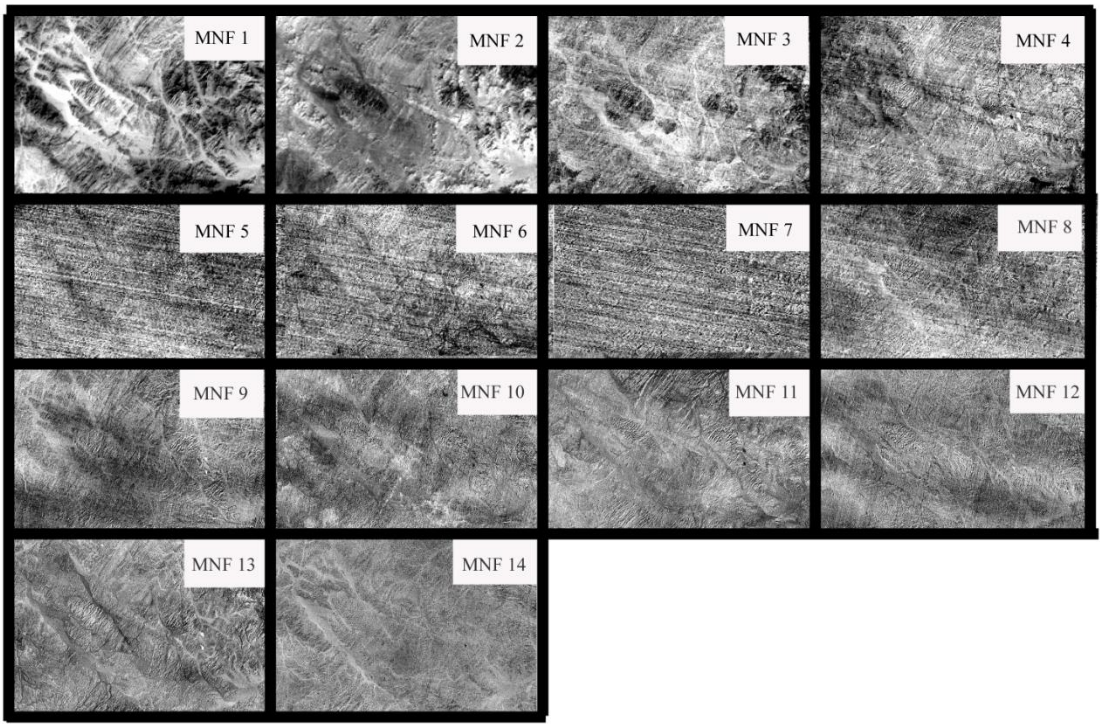

Figure 6) The MNF eigenvalues of the 14 Eigen images for the ASTER data.

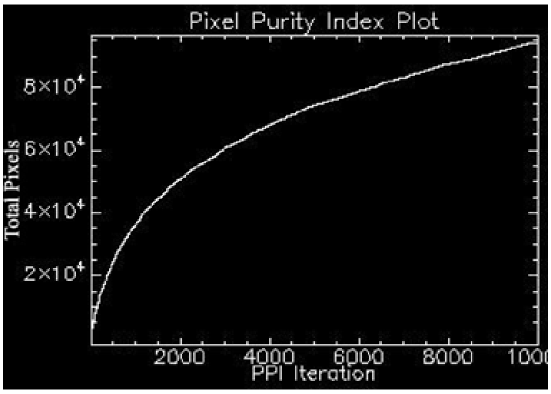

Figure 7) Pixel purity index.

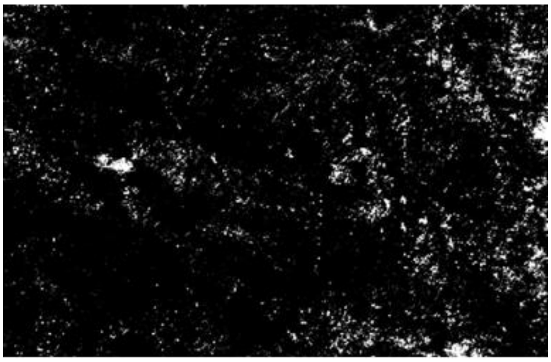

Figure 8) Pure pixel in white color.

3.4- *n*-Dimensional Visualization

The results of MNF and PPI used in the n-D visualization to locate identify and cluster the purest pixels. The pixel values of the selected eigenimages are displayed to create the *n*-dimensional feature plot. N-D visualization is applied and the purest pixels were clustered, these pure pixels were chosen to be used in the classification. The MNF transform applied to the ASTER data achieved a reasonable e separation of coherent signal from complementary noise, therefore the MNF transformed eigenimages were employed and coupled with pixel purity index and *n*-dimensional visualization technique used to facilitate the extraction of the endmember .

Six major types of rocks, riebeckite granite, quartz monzonite, granodiorite, tonalite granite, metagbbro-diorite association and metavolcanics. The profile of the spectral characterisation of these rocks are presented relative to the band numbers in Figure 9, the four image spectra derived from the *n*-dimensional endmember visualization procedure, depend on the field recogniation for rock units, so identification could be based on the adsorption value appear between wavelenght 2 to 4 for the mentioned rock units.

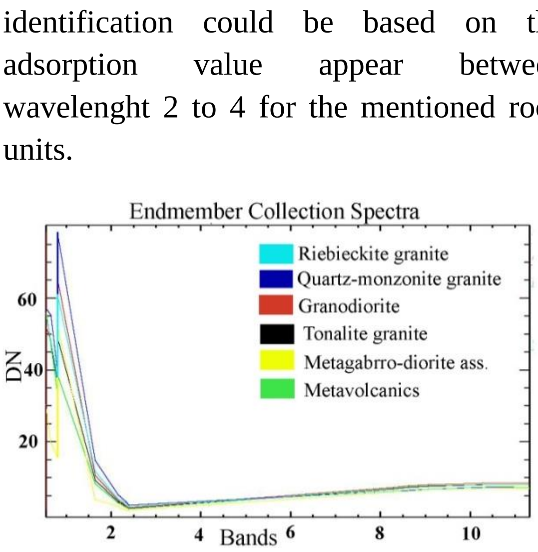

Figure 9) The spectral profile for the investigated rocks relative to the ASTER bands.

3.5- Spectral Angle Mapper (SAM)

The SAM classification method was developed by (Kurse *et al*, 1993). This type of classification is based on the spectral characteristics that evaluate similarity between end member pixel and each of the reference spectra. This similarity determined by measuring the angular variation between the pixel spectrum and the reference spectrum. Smaller angles show close matches to the reference spectrum.

According to Hegazy and El Shazly, (2000) granitoids in Ras Gharib area are clearly different in their field, petrographic and geochemical features, but they are co-magmatically related. In the study area 6 types where recognized which are different types of granites; riebeckite granite, monzogranite, tonalite granite and metagabbro-diorite association, actually all previously mentioned types are granitic type of comingling composition and of similar melting points in origin, which means that complete differentiation by classification methods will be hard to reach. (Fig. 10) shows SAM classification.

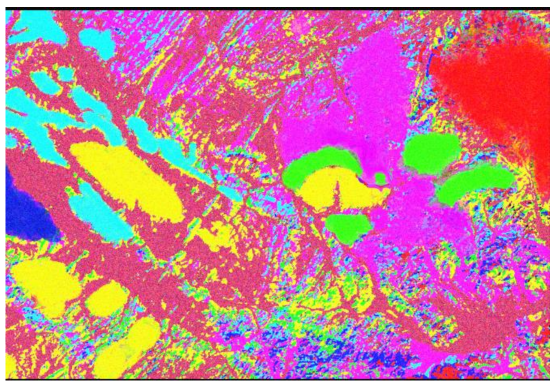

Figure 10) SAM method for Ghraib area.

3.6- Maximum Likelihood classification (MLC)

Maximum likelihood classification method assumes that the statistics for each class in each band are normally distributed and calculates the probability that a given pixel belongs to a specific class.

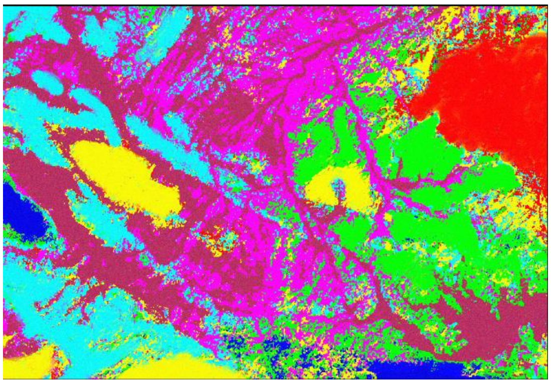

Figure 11) MLC method for Gharib area.

Unless you select a probability threshold, all pixels are classified. Each pixel is assigned to the class that has the highest probability. If the highest probability is smaller than a threshold you specify, the pixel remains unclassified. (Richards, 1999) Figure 11 shows the MLC method.

4- Band Rationing

ASTER band rationing is a widely applicable technique for geologic mapping distinguished the gossan (iron oxide minerals appear in white color), associated with massive sulfide mineralization from the host rock by ASTER (4/2) band ratio (Fig. 12); band ratio 4/5, 4/6 and 4/7 in RGB (red, green, blue) false color composites used for the discrimination of hydrothermal alteration minerals appear in white color this color are attributed to the response of bands 5 & 6 to (Al- OH) and band 7 to (Fe-OH) alteration minerals (Fig. 13).

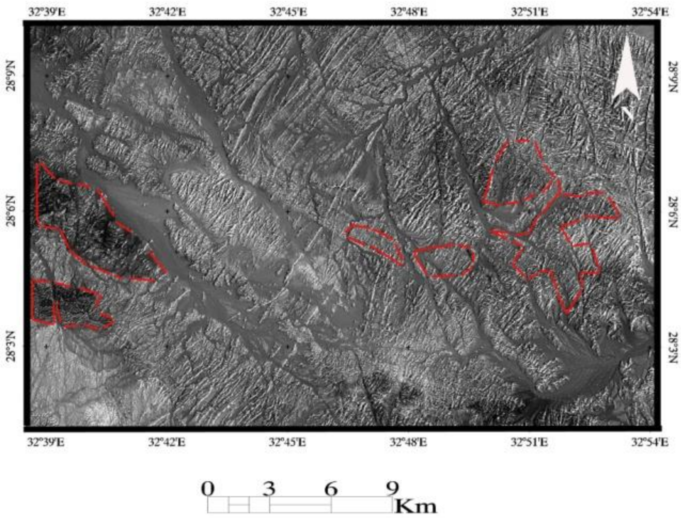

Figure 12) 4/2 altered regions (iron oxide minerals) appear in bright color.

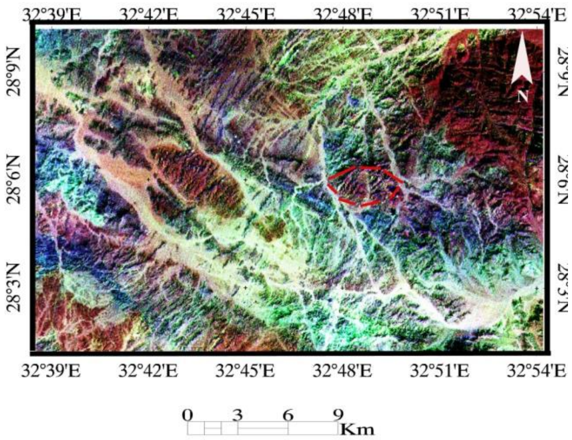

Figure 13) 4/5, 4/6 and 4/7 RGB, white color show the response of Fe-OH alteration.

Band ratio image (4/8, 4/2 and 8/9 in RGB respectively) show separation of mineralized parts of alteration zone in pinkish color (Fig. 14). Bands 4/8 (Fig. 15) show the response of iron oxides in the altered mineralized rocks. 4/2 (Fig. 12) show separation of the altered mineralized rocks from all other background materials, while 8/9 ratio used to make a better contrast for the resulting image.

The previous ASTER band ratio which applied on study area shows mineralized parts in the pinkish colored areas (Fig. 14). Sample was taken from the contact zone and analyzed by fire assay in Acme Lab in Canada to detect Au and positive result was achieved. 4/8 ratio show the iron rich parts of the alteration are considered to be main target for gold exploration (Fig. 15).

ASTER band ratio 9/8 show calcite index which present in the basic- ultrabasic rocks (Fig. 16), it clarifies positive reflectance for this index at the metaggbro- diorite association which is present in the contact with Gabel Gharib. Also calcite index appear clearly in the Metavolcanics rock unit located in the NNW of the area.

Epithermal vein deposits are characterized by two mineral assemblage; alunite (clay minerals) and Iron minerals. The ore mostly occurs in the veins, but the majority of veins are barren, the country rock is altered to the clay minerals illite, kaolinite and montmorillonite plus alunite; these assemblage of alteration minerals is known as argillic zone. ASTER band ratio 8/6 show kaolinite index, in Figure 17, positive reflectance appear in some parts of the area which indicate possibility of uranium occurrence.

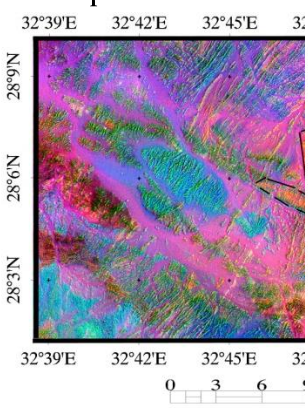

Figure 14) 4/8, 4/2 and 8/9 RGB, mineralized zone appear in pinkish color which (appear in the dased lines).

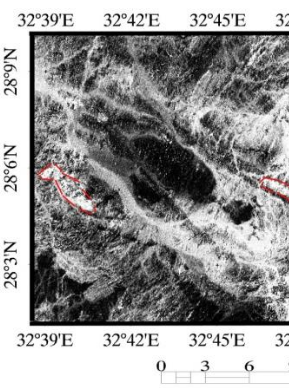

Figure 15) 4/8 white colour show response for iron oxides in altered mineralized rocks.

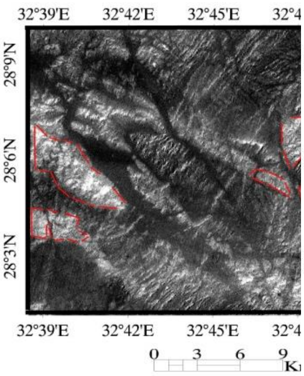

Figure 16) 9/8 shows the altered rocks from the other background in light color.

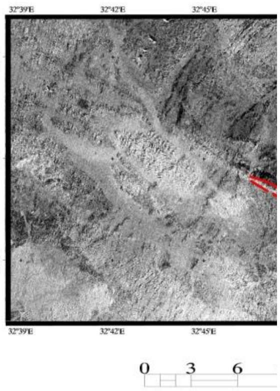

Figure 17) 8/6 shows kaolinite index positive results appear in grayish light tone.

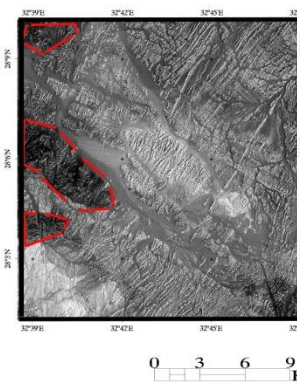

Figure 18) 5/1 show the response for opaque mafics rocks which appear in gray tone.

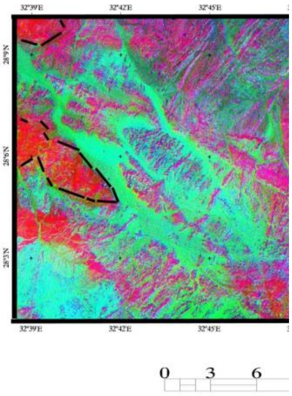

Figure 19) 5/7, 3/1 and 4/3 RGB show iron gossan appear in red color tone.

ASTER band ratio 5/1 show high expect for the rocks bearing high contents of opaque mafic rocks which generally have lower spectral reflectance than acidic, and intermediate rocks due to the high abundance of opaque phases, so we can notice that metavolcanics, gray granite and mettagabbro-diorite association which are enriched in hydroxyl- bearing phases exhibit gray color while hydroxyl free (younger granites) will exhibit light white tone (Fig. 18).

Table 2: Accuracy assessment matrcies for the two classification methods used.

(a) Classification accuracy for the Spectral Angle Mapper (**SAM**)

	Riebeckite granite	Quartz-monzonite	Granodiorite	Tonalite-granite	Metagabbro-diorite	Meta-volcanics	Total	User Acc. %
Riebeckite granite	138	42	86	30	2	1	299	46.15
Quartz-monzonite	93	212	73	24	0	0	402	52.73
Granodiorite	70	2	129	35	25	2	263	49.04
Tonalite granite	70	42	82	72	18	0	284	25.35
Metagabbro-diorite assocation	34	5	87	38	212	67	443	47.85
Metavolcanics	12	0	19	2	49	285	367	77.65
Total	417	305	476	201	306	350		50
Producer Acc. %	33.09	69.51	21.1	35.82				

(b) Classification accuracy for the Maximum Likelihood Classification (**MLH**)

	Riebeckite granite	Quartz-monzonite	Granodiorite	Tonalite granite
Riebeckite granite	396	13	17	0
Quartz-monzonite	11	289	12	0
Granodiorite	7	3	440	0
Tonalite granite	0	0	0	190
Metagabbro- diorite assocation	2	0	6	11
Metavolcanics	1	0	1	0
Total	417	305	476	201
Producer Acc. %	94.96	94.75	92.44	94.53

ASTER band ratios 5/7, 3/1 and 4/3 in RGB show the iron gossan in red color, in Figure 19, gossan is an iron- bearing capping over a sulphide deposit mostly contains the minerals pyrite, sphalerite and galena. It is formed by the oxidation and leaching of sulphide minerals leaving hydrated iron oxides such as limonite and goethite. Sulphide ore bodies are often contain gold which enriched in the oxidation zone.

5- Discussion and conclusions

The capability of the ASTER image (VNIR and SWIR bands) give good results to separate the altered and unaltered rocks and also using some methods of integrated image transformation, MNF, PPI, *n*-D, and Band Ratio to extract an accurate up to date geologic map for Gabel Gharib area. Choosing SAM and MLC in the methodology is because they are the most durable and common methods in remote sensing classification, the rock units present in the study area shown that the total of user accuracy in SAM classification are 50% while the total producer accuracy are 51.01%, in MLC total of user accuracy are 95.27%, and total of producer accuracy are 95.30%, it seems that MLC are more accurate than SAM method, but SAM method are based on spectral characteristics which give more reality results than MLC method which based on the probability, table 2; show the accuracy assessment matrices for the selected two classification methods, which show the accuracy variation between user and producer accuracy.

In user accuracy; riebeckite granite (SAM 66.84% vs 90.46% MLC), monzogranite (SAM 58.19% vs 82.29% MLC), tonalite granite (SAM 75.80% vs 78.20% MLC) and Metagabbro–diorite assocation (SAM 87.27 vs 86.04), while in producer accuracy; riebeckite granite (SAM 80.09 vs 88.16), monzogranite (SAM 68.43% vs 80.72% MLC), tonalite granite (SAM 77.38% vs 96.07% MLC) and metagabbro–diorite assocation (SAM 64.74% vs 88.09).

It is clear from the band rationing maps that the area is worthy in mineralization either in gold mineralization or uranium mineralization, the two kinds of mineralization were confirmed by geochemical analyses; from the granitic phases obtained from the area, Gharib area are called of fertile granite type, and from the band rationing maps Granitoids have been strong hydrothermally altered. Further investigation could be recommended for knowing factors affecting mineralization in the area either stratigraphic or structure factors.

Finally, it is worthy to mention that there are no mining processes found in the area even anciently, which makes this study is highly recommended for further investigation which could be a promising area.

Acknowledgments

The authors would like to thank Mr. S.G. Mehr and an anonymous reviewer for their comments that help improve the manuscript.

References

Abdel Rahman, A.M. 1990. Petrogensis of early orogenic diorites, tonalities and post orogenic trondhjemites in the Nubian Shield. Journal of petrology: 32, 1285–1312.

Abdel Rahman, A.M. 1995. Tectonic-magmatic stages of Shield evolution: the Pan-African belt of northeastern Egypt. Tectonophysics: 242, 223–240.

Abdel Rahman, A.M., Martin, R.F. 1990. The Mount Gharib A-type granite. Nubian shield: petrogenesis and role of metasomatisms at the source. Contributions to Mineralogy and Petrology: 104, 173–183.

Aboelkhair, H., Yoshiki, N., Yasushi, W., Isao, S. 2010. Processing and interpretation of ASTER TIR data for mapping of rare- metal- enriched albite granitoids in the Central Eastern Desert of Egypt. Journal of African Earth Sciences: 58, 141–151.

Beiranvand-Pour, A., Hashim, H. 2011. Application of advanced spaceborne thermal emission and reflection radiometer (ASTER) data in geologic mapping. International Journal of the Physical Sciences: 6, 7657–7668.

Boardman, J.W. 1993. Automating spectral unmixing of AVIRIS data using convex geometry concepts. In: summaries of the 4th Annual JPL Airborne Geoscience workshop, Pasadena, 11–14.

Boardman, J.W., Kruse, F.A. 1994. Automatic spectral analysis: a geological example using AVIRIS data, North Grapevine mountain, Nevada. In: 10th thematic conference on geologic remote sensing, Ann. Arbor, pp. 407-418.

Boardman, J.W., Kruse, F.A., Green, R.O. 1995. Mapping target signatures via partial un mixing of AVIRIS data: in summaries, Fifth JPL Airborne Earth Science workshop, JPL publication 95-1, 23–26.

Burke, K., Sengor, C. 1986. Tectonic escape in the evolution of the continental crust. AGU Geodynamic Series: 14, 41–53.

Di Tommaso, I., Rubinstein, N. 2007. Hudrothermal alteration mapping using ASTER data in the linfiernillo porphyry deposit, Argentina. Ore Geology Reviews: 32, 275–290.

El-Sayed Zeinelabdein, K.A. 2009. Sudan experience in using remote sensing for minerla prospecting, Fac. of Petroleum and minerals, Alneelain Univ., Khartoum, Sudan, pp. 636-646.

Gharieb, A.G.N. 2010. Rock discrimination using spectral analysis techniques of remote sensing data, Egypt: A case study. Fifth International Conference on the Geology of the Tethys Realm, South Valley University, January 2010, P. 297-306.

Gulam, A., Kusky, T.M. 2010. Mineral exploration and altration zone mapping in eastern Desert of Egyp using ASTER data. ASPRS 2010 annual Conference.

Harasanyi, J.C. 1993. Detection and classification of subpixel spectral signatures in hyperspectral image sequences. Unpublished Ph.D. thesis, university of Maryland, 116pp.

Hegazy, H.A., El-Shazly, S.M. 2000. West Ras Gharib granitoids, Eastern Desert, Egypt an example for Neoproterozoic magmatic arc. Bulletin of Faculty of Sciences, Assuit University: 29, 29–50.

Hume, M.E. 1937. Geology of Egypt, Volume II, part II. Geologic survey of Egypt.

Jensen, J.R., 2005: Introduction digital image processing. Prentice Hall, upper saddle river, 256p.

Kroner, A., Greiling, R.O., Reischmann, F., Hussien, I.M., Stern, R.J., Durr, S., Druger, J., Zimmer, M. 1987. Pan-African crustal evolution in the Nubian segment of northeast Africa. In Kroner, A. (ed): Proterozoic lithospheric evolution. American Geophysical Unioin, Washington D.C, pp. 235–257.

Mars, J.C., Rowan, L.C. 2006. Regional mapping pf phyllic- and argillic altered rocks in the Zagros magmatic arc. Iran, using advanced spaceborne thermal emission and reflection radiometer (ASTER) data and logical operator algorithms. Geoshpere: 2, 161–186.

Massironi, M.L., Bertoldi, P., Calafa, D., Visona, B. 2008. Interpretation and processing of ASTER data for geologic mapping and granitoids detection in the saghro massif (eastern Anti- Atlas, Morocco). Geoshpere: 4, 736–759.

Mohamed, F.H., Moghazy, A.M., Hassanen, M.A. 1999. Petrogenesis of late Proterozoic granitiods in the Ras Gharib magmatic province, northern Eastern Desert, Egypt: petrological and geochemical constraints. Neues Jahrbuch Fur Mineralogie-Abhandlungen: 174, 319–353.

Ninomiya, Y., 2003: A stabilized vegetation index and several mineralogic indices defined for ASTER VNIR and SWIR data. Proc. IEEE 2003 International Geoscience and Remote Sensing Symposium (IGARSS'03) v.3, Toulouse, France, 21–25 July 2003, pp. 1552–1554.

Noweir, A.M., Sewifi, B.M., Abu El Ela, M. 1990. Geology, petrography, Geochemistry and petrogensis of the Egyptian younger granites. Qatar University Science Bulletin: 10, 363–393.

Rajesh, H.M. 2004. Application of remote sensing and GIS in mineral resource mapping- An overview, Journal of Mineralogical and Petrological Science: 99, 83–103.

Richards, J.A., 1999. Remote Sensing Digital Image Analysis, Springer-Verlag, Berlin, pp. 240.

Rowan, L.C., Robert, G.S., John, C. 2006. Distribution of hydrothermally altered rocks in the Reko Diq, Pakistan mineralized area based on spectral analysis of ASTER data. Remote Sensing of Environment: 104, 74–87.

Rowan, L.C., Mars, J.C. 2003. Lithologic mapping in the Mountain Pass, California area using Advanced Spaceborne Thermal Emission and Reflection Radiometer (ASTER) data. Remote Sensing of Environment: 84, 350–366.

Sanjeevi, S. 2008. Targeting limestone and bauxite deposits in Southern India by spectral unmixing of hyperspectral image data. The International Archives of the Photogrammetry, Remote Sensing and Spatial Information Sciences: 37, B8. Beijing 2008.

Stern, R.J. 1994. Arc assembly and continental collision in the Neoproterozoic east Africa Orogen: implications for the consolidation of Gondwanaland. Annual review of Earth and Planetry Sciences: 22, 319–351.

Urug, R. 1997. Rodinia to Gondwana the Geodynamic map of Gondwana supercontinent assembly. GSA Today: 7, 1–6.

Windely, B. 1992. Proterozoic collisional and accretinary orogens. In Condie, K.C. (ed.): Proterozoic crustal evolution, Elsevier, Amsterdam, pp. 419-446.

Yamaguchi, Y.I., Fujisada, H., Kudoh, M., Kawakami, T., Tsu, H., Kahle, A.B., Pniel, M., 1999. ASTER instrument characterization and operation scenario. Advances in Space Research: 23, 1415–1424 .

Zhang, X., Pazner, M., Duke, N. 2007. Lithologic and mineral information extraction for gold exploration using ASTER data in the south chocolate mountains (California). photogrammetry and remote sensing: 63, 271–282.